Optik - International Journal for Light and Electron Optics 239 (2021) 166680

Contents lists available at ScienceDirect

Optik

journal homepage: www.elsevier.com/locate/ijleo

Original research article

Electronic band structure, elastic, optical and thermodynamic characteristic of cubic YF_3: An ab initio study

Mohamed Amine Ghebouli [a,b,**], Brahim Ghebouli [c], Tayeb Chihi [d], Messaoud Fatmi [b], Rabah Khenata [e,*], Hamad Rahman Jappor [f,*], Saleh H. Naqib [g]

[a] Department of Chemistry, Faculty of Technology, University of Mohamed Boudiaf, M'sila, 28000, Algeria
[b] Research Unit on Emerging Materials (RUEM), University of Setif, 19000, Algeria
[c] Laboratory of Studies Surfaces and Interfaces of Solids Materials, Department of Physics, Faculty of Science, University Ferhat Abbas of Setif, Setif, 19000, Algeria
[d] Laboratory for Developing New Materials and Their Characterization, Department of Physics, Faculty of Science, University of Setif, 19000, Algeria
[e] Laboratoire de Physique Quantique de la Matière et de la Modélisation Mathématique (LPQ3M), Faculté des Sciences, Université de Mascara, Mascara, 29000, Algeria
[f] Department of Physics, College of Education for Pure Sciences, University of Babylon, Hilla, Iraq
[g] Department of Physics, University of Rajshahi, Rajshahi, 6205, Bangladesh

ARTICLE INFO

Keywords:
Yttrium fluoride
DFT
Optoelectronics properties
Thermodynamic properties

ABSTRACT

We have calculated the bond lengths $d_{F3\rightarrow F5,7,8}$, $d_{F4\rightarrow F5,6,8}$, $d_{F2\rightarrow F5,7,8}$, $d_{F1\rightarrow F6,7,8}$, $d_{F1\rightarrow 8-Y1,2,3}$, $d_{F9\rightarrow Y1,2,3}$, $d_{F1\rightarrow 8-F9}$ and single-crystal elastic stiffness constants, C_{ij} and polycrystalline elastic moduli at different pressures by using GGA-PBE, GGA-PBESOL and LDA approach for cubic YF_3. Yttrium fluoride is found to be elastically stable in the pressure range 0–40 GPa. Shear modulus, linear compressibility and Poisson's ratio have maximum and minimum values along with different crystallographic directions, which explain their predicted anisotropy. The direct Γ-Γ band gap value 5.082 eV indicates towards the insulating character of YF_3. The broad band gap is a sign that this compound should function as an emission center. We predicted the first and second-order pressure coefficients of direct and indirect band gaps using the GGA-PBE, GGA-PBESOL and LDA approaches. The estimated volumetric thermal expansion coefficient, constants volume and constant pressure heat capacities and entropy at zero pressure and 300 K are $1.66 \times 10^5\ K^{-1}$, 82.56 $Jmol^{-1}K^{-1}$ and 83.59 $mol^{-1}\ K^{-1}$, respectively. The edge of the optical absorption is located at 48.5 nm which is caused by the V_1-C_1 transition at the Γ point in the Brillouin zone that corresponds very well to the direct band gap at Γ- Γ.

1. Introduction

The rare earth elements and yttrium are important materials in electronic equipment industry. They are also used in defense, energy and communications industries. Yttrium trifluoride, YF_3, is an inorganic chemical compound and which is not found naturally in pure form. Yttrium fluoride is used in metallic yttrium, thin films, glasses and ceramics [1]. Some experimental researches were

* Corresponding authors.
** Corresponding author at: Department of Chemistry, Faculty of Technology, University of Mohamed Boudiaf, M'sila, 28000, Algeria.
E-mail addresses: mohamedamine.ghebouli@univ-msila.dz (M.A. Ghebouli), rabah_khenata@univ-mascara.dz (R. Khenata), hrjms@yahoo.com (H.R. Jappor).

https://doi.org/10.1016/j.ijleo.2021.166680
Received 27 January 2021; Accepted 4 March 2021
Available online 8 March 2021

Table 1
The calculated equilibrium lattice constant a_0 (Á), bulk modulus B^0 (GPa), the pressure derivative of bulk modulus $B_0^{'}$ and bonds lengths (Á),$d_{F3\rightarrow F5,F7,F8}$, $d_{F4\rightarrow F5,F6,F8}$, $d_{F2\rightarrow F5,F7,F8}$, $d_{F1\rightarrow F6,F7,F8}$, $d_{F1\rightarrow F8-Y12,3}$, $d_{F9\rightarrow Y12,3}$ and $d_{F1\rightarrow F8-F9}$ for YF_3 by using GGA-PBE, GGA-PBESOL and LDA.

Parameter	*GGA − PBE*	*GGA − PBESOL*	*LDA*	Other
a_0	5.593	5.535	5.227	5.385 [16]
B_0	89.443	101.53	120.61	
$B^{'}$	5.013	4.85	4.384	
$d_{F3-F5,7,8}$	2.71607	2.76776	2.52602	
$d_{F4-F5,6,8}$	2.71607	2.76776	2.52602	
$d_{F2-F5,7,8}$	2.71607	2.76776	2.52602	
$d_{F1-F6,7,8}$	2.71607	2.76776	2.52602	
$d_{F1\rightarrow 8-Y1,2,3}$	2.44650	2.42469	2.28984	
$d_{F9-Y1,2,3}$	2.79697	2.76776	2.61359	
$d_{F1\rightarrow 8-F9}$	2.49231	2.47669	2.33928	

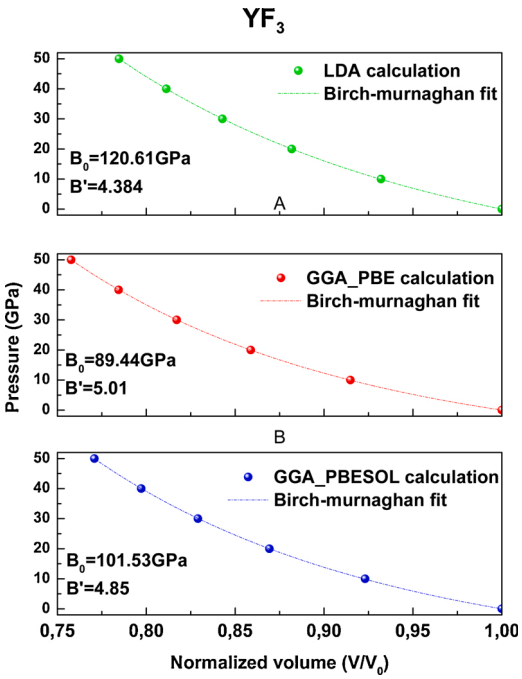

Fig. 1. The normalized volume versus pressure for YF_3.

carried out, such as by D.F. Bezuidenhout et al. which investigated the optical, structural and chemical properties of yttrium fluoride thin films [1]. The synthesis of YF_3 was done by the dry method. Miao Wang et al. prepared crystalline particles of YF_3 from a simple solution with various fluorite sources (NH_4F, HF, NH_4F-HF) and a molar ratio of Y^{3+}/F^{-} at room temperature [2]. Xiaoliang Yang et al. studied the YF_3 nanoparticles and suggested that the luminescence may be ascribed to the difference in the Y—F bond nature in YF_3 [3]. Furthermore, Nafziger et al. established that YF_3 is a candidate for potential use as fluxes for electroslag melting reactive metals [4]. All these studies indicate that YF_3 has significant prospect to be used in a variety of materials and optoelectronics sectors.

We have used the pseudo-potential plane-wave (PP-PW) method within the generalized gradient approximation (GGA-PBE, GGA-PBESOL) and local density approximation (LDA) to determine the structural, elastic, electronic, optical and thermodynamic properties of YF_3 in this work. Investigation and understanding of these physical properties are essential to unlock the full potential of a compound for future applications. This is the prime motivation of this paper. The remainder of the manuscript is structured as follows. The computational methodology is given in Section 2. The computed results and relevant discussions are presented in Section 3. A conclusion of the present investigation is reported in Section 4.

2. Methodology

The theoretical results have been obtained using ab initio calculations, based on pseudo-potential plane-wave (PP-PW) density

Table 2
The predicted elastic constants (GPa), bulk modulus (GPa) and their pressure derivatives at equilibrium by using GGA-PBE, GGA-PBESOL and LDA for YF_3.

Computational scheme	C_{11}	C_{12}	C_{44}	B	$\frac{\partial C_{11}}{\partial P}$	$\frac{\partial C_{12}}{\partial P}$	$\frac{\partial C_{44}}{\partial P}$	$\frac{\partial B}{\partial P}$
GGA − PBE	141.43	65.75	47.58	90.98	5.517	3.751	1.15	4.94
GGA − PBESOL	150.34	73.58	52.73	99.17	5.682	3.791	0.992	4.72
LDA	193.74	77.61	58.99	116.32	5.463	3.363	0.825	4.28

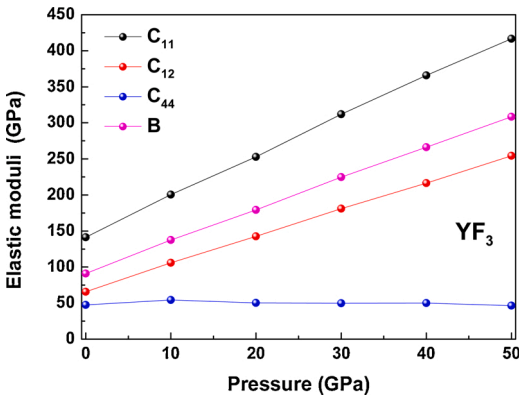

Fig. 2. Elastic stiffness constants and bulk modulus of YF_3 as a function of pressure.

functional theory (DFT) as implemented in the CASTEP code [5]. The interactions of valence electrons with ion cores in reciprocal space are treated via the Vanderbilt-type ultrasoft pseudo-potential [6]. The generalized gradient approximations (GGA-PBE, GGA-PBESOL) of Perdew, Burke and Ernzerhof [7] and the local density approximation (LDA) of Teter and Pade [8] describe the exchange and correlation potentials. We used cut-off energy of 360 eV with a reciprocal space sampling grid of size $8 \times 8 \times 8$ k-points generated through the Monkhorst-Pack scheme [9]. We have optimized the lattice constant at a fixed volume of the unit cell which corresponds to the minimum energy. The structural parameters were determined using the Broyden–Fletcher–Goldfarb–Shanno minimization technique [10], which provides with a fast way to find the lowest energy crystal structure. The study of the thermodynamic properties was carried out by the quasi-harmonic Debye model (QHDM) as implemented within the Gibbs program. The essential features of the QHDM and their elaboration can be found in [11–15].

3. Results and discussion

3.1. Structural analysis

Yttrium fluoride crystallizes in cubic structure with space group $Pm\overline{3}m(221)$. The atomic positions in the unit cell are- Y: 1a (0, 0, 0) and F: 3d (1/2, 0, 0). We have reported in Table 1 the equilibrium lattice constant a_0 and bond lengths $d_{F3\rightarrow F5,7,8}$, $d_{F4\rightarrow F5,6,8}$, $d_{F2\rightarrow F5,7,8}$, $d_{F1\rightarrow F6,7,8}$, $d_{F1\rightarrow 8-Y1,2,3}$, $d_{F9\rightarrow Y1,2,3}$, $d_{F1\rightarrow 8-F9}$, by using GGA-PBE, GGA-PBESOL and LDA approach. Our computed lattice constants are in agreement with those quoted in the literature [16]. We show in Fig. 1 the normalized volume as a function of pressure using GGA-PBE, GGA-PBESOL and LDA. The obtained results of bulk modulus B^0 and its pressure derivative $B_0^{'}$ by using the fitting scheme $P(V/V_0)$ are listed in Table 1. There are no available experimental and theoretical data for the other structural parameters, and therefore, our results are to be treated as predictions. The analysis of bond lengths implies that $d_{F3\rightarrow F5,F7,F8}$, $d_{F4\rightarrow F5,F6,F8}$, $d_{F2\rightarrow F5,F7,F8}$ and $d_{F1\rightarrow F6,F7,F8}$ are octahedral distances and have identical values for the same approach. This value increases in the sequence of $LDA \rightarrow GGA - PBE \rightarrow GGA - PBESOL$. While the non-identical bond lengths $d_{F1\rightarrow F8-Y12,3}$, $d_{F9\rightarrow Y12,3}$ and $d_{F1\rightarrow F8-F9}$ naturally differ for the same approach and increase in the sequence of $LDA \rightarrow GGA - PBESOL \rightarrow GGA - PBE$.

3.2. Elastic constants

The compound under study possesses cubic symmetry. Therefore, there are three independent single-crystal elastic stiffness constants, namely, C_{11}, C_{12} and C_{44}. The computed values of C_{ij} for YF_3 using GGA-PBE, GGA-PBESOL and LDA are reported in Table 2. The polycrystalline bulk modulus B and its pressure derivative $\frac{\partial B}{\partial P}$ calculated from elastic constants have nearly the same value as obtained from the fitting scheme $P(V/V_0)$. This confirms the accuracy of our calculations of elastic constants. The generalized elastic stability criteria for a cubic crystal under pressure are [17]:

Table 3
The bulk modulus, shear modulus, Young's modulus, Poisson's ratio and universal anisotropy factor with GGA-PBE, GGA-PBESOL and LDA for YF_3.

Scheme	B			G			E_H	σ_H	A_U
	B_V	B_R	B_H	G_V	G_R	G_H			
GGA-PBE	90.98	90.98	90.98	43.689	43.142	43.415	112.37	0.294	0.0633
GGA-PBESOL	99.17	99.17	99.17	46.99	45.87	46.43	120.49	0.297	0.1222
LDA	116.32	116.32	116.32	58.62	58.62	58.62	150.57	0.284	0.0003

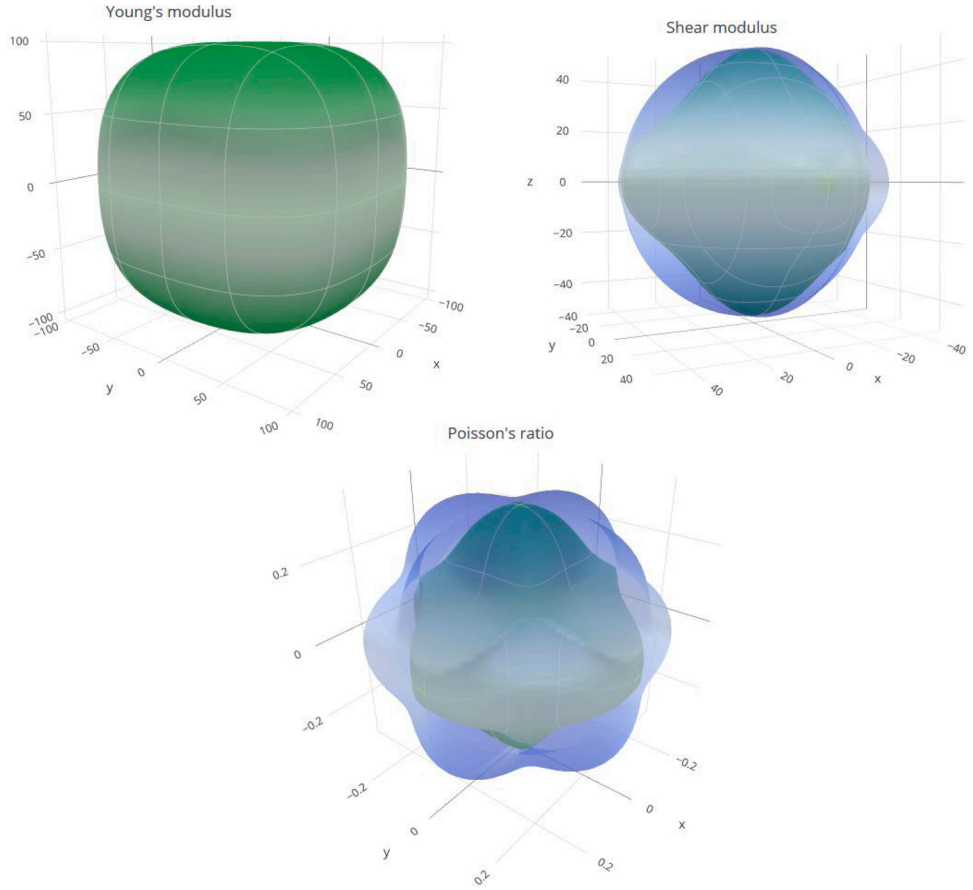

Fig. 3. The direction dependent of Young's modulus, shear modulus and Poisson's ratio for YF_3.

Table 4
The predicted direction-dependent Young's modulus, linear compressibility, shear modulus and Poisson's ratio within GGA-PBE, GGA-PBESOL and LDA schemes for YF_3.

Scheme	Young's modulus		Linear compressibility		Shear modulus		Poisson's ratio	
	E_{min}	E_{max}	β_{min}	β_{max}	G_{min}	G_{max}	σ_{min}	σ_{max}
GGA-PBE	99.69	121.57	3.6638	3.6638	37.839	47.589	0.2108	0.2108
GGA-PBESOL	101.98	134.39	3.3611	3.3611	38.377	52.739	0.1803	0.4012
LDA	149.35	151.4	2.8656	2.8656	58.066	58.997	0.2787	0.2889

$$C_{11} + 2C_{12} > 0, C_{44} > 0, C_{11} - C_{12} > 0, C_{12} < B < C_{11} \quad (1)$$

The computed elastic stiffness constants fulfil the above criteria at ambient conditions and under pressure; therefore, the compound YF_3 is elastically stable. The effect of pressure on elastic parameters is shown in Fig. 2. They increase monotonously when the pressure is enhanced, except C_{44} which is quite insensitive to the pressure. We reported in Table 3 the bulk modulus, shear modulus, Young's

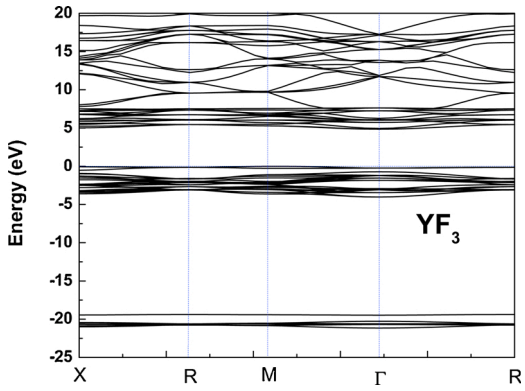

Fig. 4. The electronic band structure of YF_3 at equilibrium geometry along high symmetry directions X, R, M and Γ in the Brillouin zone.

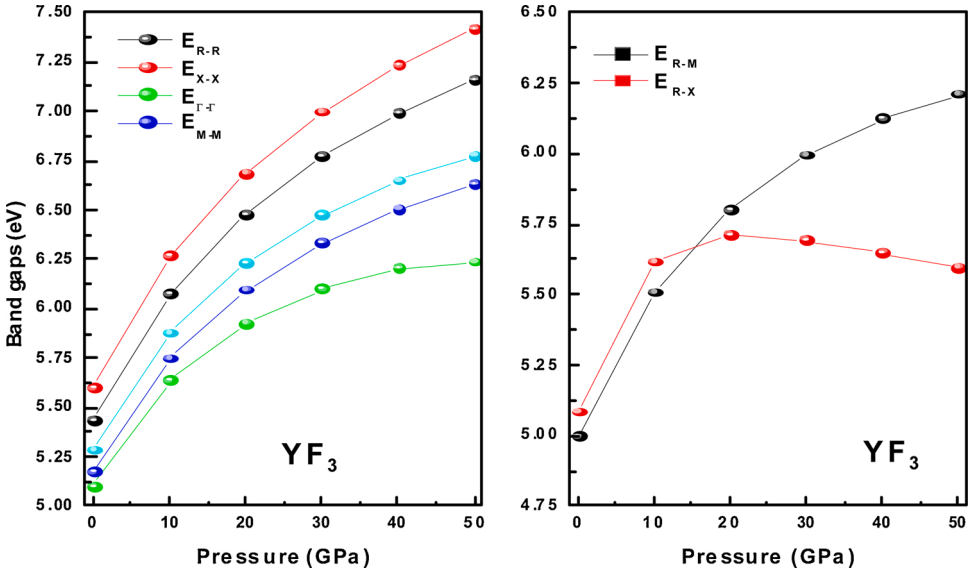

Fig. 5. The direct and indirect band gaps for YF_3 at different pressures.

modulus, Poisson's ratio and anisotropy factor calculated from elastic constants using Voigt [18], Reuss [19] and Hill [20] approximations. The Poisson's ratio is greater than the limiting value of 0.25, and the mechanical behavior of this material is expected to be dominated by covalent bonding [21]. The value of the anisotropy factor is unity indicating that YF_3 is mechanically isotropic. This is expected for cubic crystals. We illustrated in Fig. 3 the direction-dependent Young's modulus, shear modulus and Poisson's ratio in 3D using the ELATE software [22]. The minimum and maximum of each parameter are shown by green and blue colors, respectively. The isotropic material shows a spherical shape and any distortion from this shape indicates the anisotropy. Young's modulus tends to be isotropic, while, shear modulus and Poisson's ratio are anisotropic. We listed the predicted maximum and minimum values in Table 4.

3.3. Electronic properties

We have plotted in Fig. 4 the electronic band structure of YF_3 at equilibrium geometry along the high symmetry direction X, R, M and Γ in the Brillouin zone using the GGA-PBE approach. YF_3 compound exhibit a direct band gap $E_{\Gamma-\Gamma}$ of the value of 5.082 eV. This material is a direct band gap insulator. This value of the band gap is in reasonable agreement with theoretical value of, 5.617 eV cited in the literature [16]. There are two distinct valence bands in the region −25 eV to −0 eV. The upper valence band is located between -4.02 eV and the Fermi level. The first conduction band started at 5.72 eV above the Fermi level. The wide band gap is a sign that this compound can act as an emission center. We display in Fig. 5 the predicted direct and indirect band gaps as a function of pressure in the GGA-PBE approximation. They increase monotonously when the pressure is raised in the range 0–40 GPa. We have calculated the first and second-order coefficients of direct and indirect band gaps using GGA-PBE, GGA-PBESOL and LDA approach. These gaps, as a function of pressure, follow the equation given by $E(p) = E_0 + \frac{\partial E}{\partial P}P + \frac{\partial^2 E}{\partial P^2}P^2$. We listed E_0, $\frac{\partial E}{\partial P}$, $\frac{\partial^2 E}{\partial P^2}$ in Table 5 for all the band gaps. Fig. 6 shows the total and partial density of states (TDOS and PDOS, respectively) of YF_3 for the GGA-PBE scheme. The upper valence band

Table 5

The predicted direct and indirect band gaps E_0, $\frac{\partial^2 E}{\partial P^2}$ and $\frac{\partial E}{\partial P}$ between various points of symmetry in the Brillouin zone within GGA-PBE, GGA-PBESOL and LDA for YF_3.

Scheme	Parameter	E_{R-X}	E_{R-M}	$E_{R-\Gamma}$	E_{R-R}	E_{X-X}	$E_{\Gamma-\Gamma}$	E_{M-M}
	E_0	5.169	5.431	5.596	5.597	5.097	5.082 5.617 [18]	5.282
$GGA-PBE$	$\frac{\partial^2 E}{\partial P^2}(\times 10^{-4})$	−5.272	−5.540	−4.956	−5.640	−5.824	−6.207	−5.478
	$\frac{\partial E}{\partial P}(\times 10^{-2})$	5.440	6.107	4.799	6.331	5.075	3.859	5.602
	E_0	5.342	5.134	5.134	5.823	5.261	5.234	4.971
$GGA-PBESOL$	$\frac{\partial^2 E}{\partial P^2}(\times 10^{-4})$	−4.632	−7.037	−3.990	−5.506	−5.400	−4.618	−6.963
	$\frac{\partial E}{\partial P}(\times 10^{-2})$	4.843	7.729	3.995	6.033	4.477	2.563	7.188
	E_0	6.311	6.630	6.004	7.049	6.233	6.168	6.453
LDA	$\frac{\partial^2 E}{\partial P^2}(\times 10^{-4})$	−3.424	−3.662	−3.156	−3.845	−3.479	−4.728	−3.657
	$\frac{\partial E}{\partial P}(\times 10^{-2})$	4.267	4.645	3.461	5.064	3.738	3.474	4.199

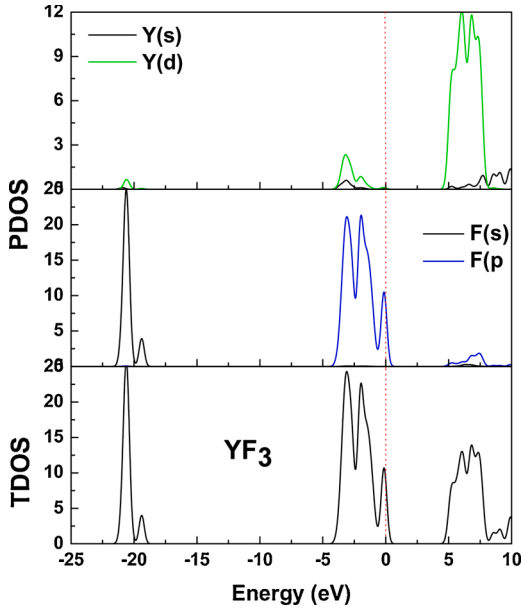

Fig. 6. Total and partial density of states for YF_3.

located in the range (-4.14 eV to E_F) is due to the F: p electronic state with a small contribution from Y: d orbital. The first conduction band in the energy range E_F to 4.51 eV is empty. Consequently, the electronic transition may occur between F: p and Y: d or Y: s states. The hybridization between F: p and Y: d orbitals in the upper valence band confirms the covalent bonding character between the atomic states F: p and Y: d.

3.4. Optical properties

The optical constants as a function of the energy of the incident electromagnetic wave were calculated using the photon induced matrix elements of electronic transitions between different energy states [23]. We have displayed an imaginary part of dielectric function versus photons energy in Fig. 7 (right panel). The transition energy $E(k) = E_{cj}(k) - E_{vi}(k)$ is plotted in Fig. 7 (left panel); where v_i and c_j are the valence band number i and the conduction band number j respectively. The threshold energy of the dielectric function occurs at 5.15 eV, which corresponds to the fundamental direct band gap $E_{\Gamma-\Gamma}$ for YF_3. We study transitions from occupied states F-p (valence band) to unoccupied states (conduction band) Y-d or Y-s. One can notice that all possible transitions are reported in Table 6. We have plotted the loss function, reflectivity and absorption spectra versus wavelength in Fig. 8. The loss function is characterized by multiple peaks. The high energy peaks are located at 51 nm and 62 nm after the ionization edge. The other and the most intense peak is located at 104 nm. This peak at 104 nm defines the plasma energy at which both reflectivity and absorption coefficient fall sharply. The

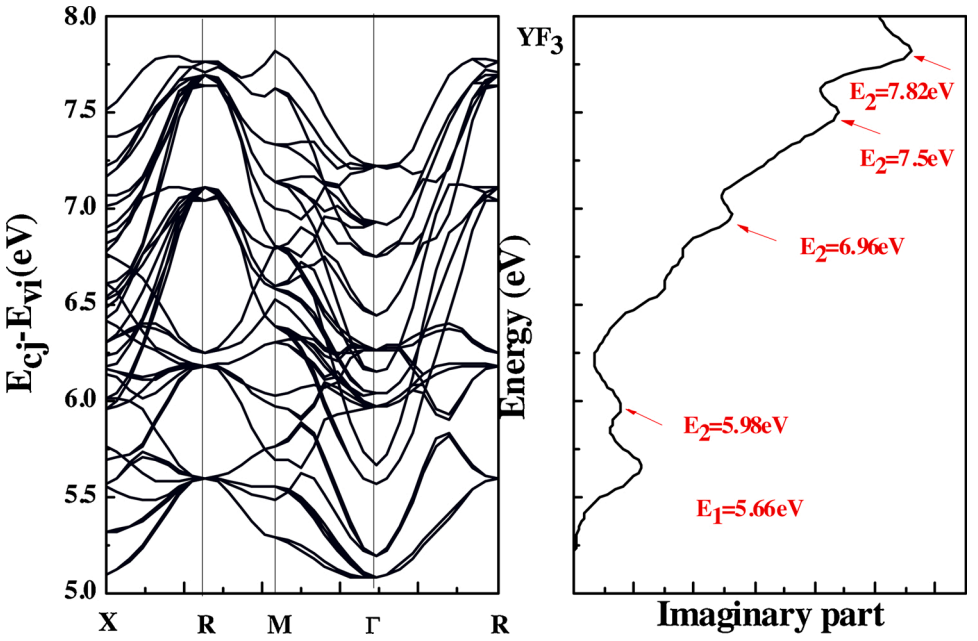

Fig. 7. Transition energy $E(k) = E_{Cj}(k) - E_{Vi}(k)$ (left panel) and imaginary part of the dielectric constant (right panel) for YF_3.

reflectivity of YF_3 is low. It reached a maximum value of only 0.47 at 112 nm. It is reported that the lower reflectivity indicates the higher UV or visible light absorption [24]. The highest value of absorption is 225486 cm^{-1} at a wavelength of 122 nm. The higher absorption value indicates that YF_3 is a potential candidate as a photocatalyst. On can see that the maximum of absorption corresponds to the maximum of reflectivity where the loss function is very small.

3.5. Thermodynamic properties

The thermodynamic properties were studied as functions of temperature and pressure by applying the quasi-harmonic Debye approximation. We present in Fig. 9 the volume temperature diagram of YF_3 at several pressures. The volume increases with increasing temperature at a given pressure. On the other side, as the pressure increases the volume decreases at a given temperature. Fig. 10 shows the temperature effect on bulk modulus at a given pressure. The compressibility decreases with increasing temperature at a given pressure and increases with increasing pressure at a given temperature. The bulk modulus is 117.22 GPa at 300 K and zero pressure. Fig. 11 displays the dependence of the Debye temperature θ_D on temperature. The Debye temperature is practically constant between

Table 6
All the electronic transitions between five high valence bands and five low lying conduction bands.

Energy	$X \rightarrow R$	$M \rightarrow \Gamma$	$\Gamma \rightarrow R$
$E = 5.66eV$	$V_5 \rightarrow C_1$, $V_4 \rightarrow C_1$, $V_3 \rightarrow C_1$, $V_2 \rightarrow C_1$, $V_1 \rightarrow C_1$	$V_1 \rightarrow C_3$, $V_2 \rightarrow C_1$, $V_2 \rightarrow C_3$, $V_2 \rightarrow C_2$, $V_4 \rightarrow C_1$, $V_4 \rightarrow C_2$ $V_3 \rightarrow C_2$, $V_5 \rightarrow C_1$, $V_5 \rightarrow C_2$	$V_1 \rightarrow C_3$, $V_3 \rightarrow C_1$, $V_3 \rightarrow C_3$, $V_5 \rightarrow C_1$, $V_5 \rightarrow C_3$
$E = 5.98eV$	$V_3 \rightarrow C_5$, $V_6 \rightarrow C_4$, $V_4 \rightarrow C_4$, $V_5 \rightarrow C_3$, $V_5 \rightarrow C_1$, $V_2 \rightarrow C_5$, $V_5 \rightarrow C_4$, $V_4 \rightarrow C_1$,$V_4 \rightarrow C_2$, $V_5 \rightarrow C_2$	$V_6 \rightarrow C_3$, $V_6 \rightarrow C_4$, $V_6 \rightarrow C_6$ $V_6 \rightarrow C_5$, $V_5 \rightarrow C_6$, $V_3 \rightarrow C_6$ $V_5 \rightarrow C_5$	$V_6 \rightarrow C_6$, $V_5 \rightarrow C_6$ $V_3 \rightarrow C_6$, $V_1 \rightarrow C_6$ $V_3 \rightarrow C_6$, $V_1 \rightarrow C_4$
$E = 6.96eV$	$V_6 \rightarrow C_3$, $V_5 \rightarrow C_7$, $V_4 \rightarrow C_7$ $V_6 \rightarrow C_6$, $V_5 \rightarrow C_6$, $V_5 \rightarrow C_6$ $V_4 \rightarrow C_6$, $V_1 \rightarrow C_7$	$V_6 \rightarrow C_6$, $V_1 \rightarrow C_7$, $V_5 \rightarrow C_6$ $V_3 \rightarrow C_6$	$V_5 \rightarrow C_6$, $V_6 \rightarrow C_6$ $V_3 \rightarrow C_7$, $V_1 \rightarrow C_7$
$E = 7.5eV$	$V_6 \rightarrow C_7$, $V_5 \rightarrow C_7$	$V_6 \rightarrow C_7$, $V_2 \rightarrow C_7$, $V_5 \rightarrow C_7$ $V_1 \rightarrow C_7$	$V_5 \rightarrow C_7$, $V_3 \rightarrow C_7$ $V_1 \rightarrow C_7$
$E = 7.82eV$	$V_6 \rightarrow C_7$, $V_5 \rightarrow C_7$	$V_6 \rightarrow C_7$, $V_2 \rightarrow C_7$, $V_5 \rightarrow C_7$ $V_1 \rightarrow C_7$	$V_5 \rightarrow C_7$, $V_3 \rightarrow C_7$ $V_1 \rightarrow C_7$

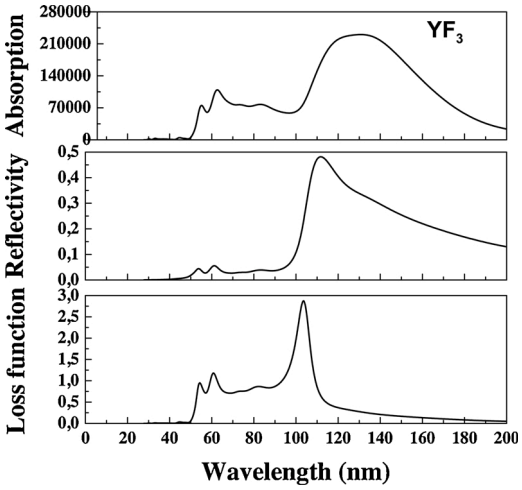

Fig. 8. The absorption coefficient, reflectivity and loss function versus wavelength for YF_3.

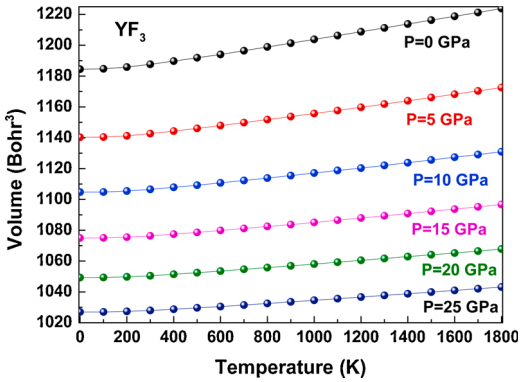

Fig. 9. The volume temperature diagram of YF_3 at different pressures.

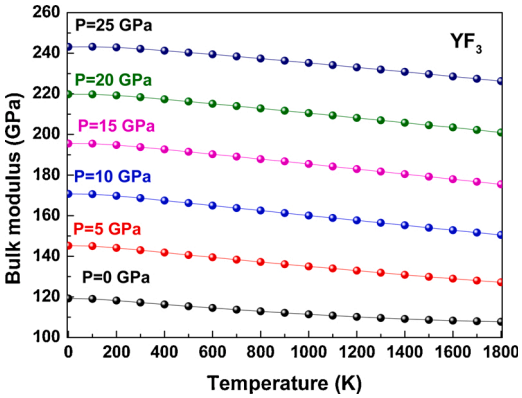

Fig. 10. The temperature effect on bulk modulus for YF_3 at different pressures.

0 and 300 K, and then it decreases linearly with increasing temperature. The Debye temperature at zero pressure and 300 K is 477.4 K. Fig. 12 shows the temperature effect on volumetric thermal expansion coefficient. It increases sharply when the temperature rises to 500 K. When $T > 500$ K, the volumetric thermal expansion coefficient approaches to a linear increase and this variation is less sensitive to the temperature. The volumetric thermal expansion coefficient is 1.66×10^5 K^{-1} at 300 K and zero pressure. Figs. 13 and 14

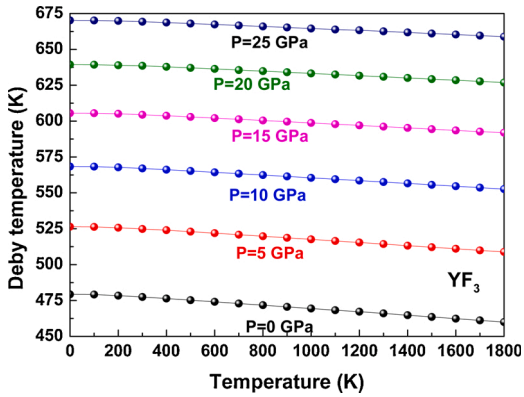

Fig. 11. The Debye temperature as a function of temperature for YF_3 at different pressure.

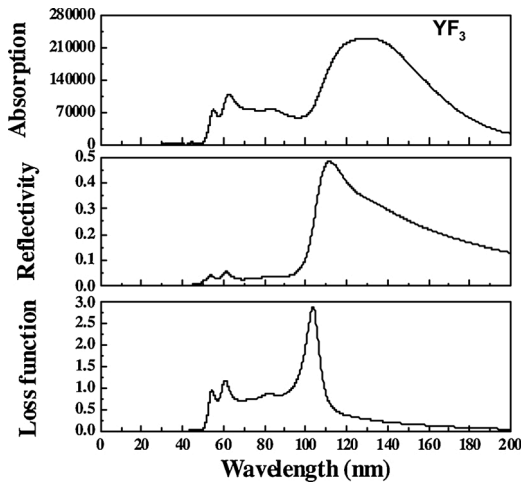

Fig. 12. The effect of temperature on the thermal expansion coefficient for YF_3 at different pressures.

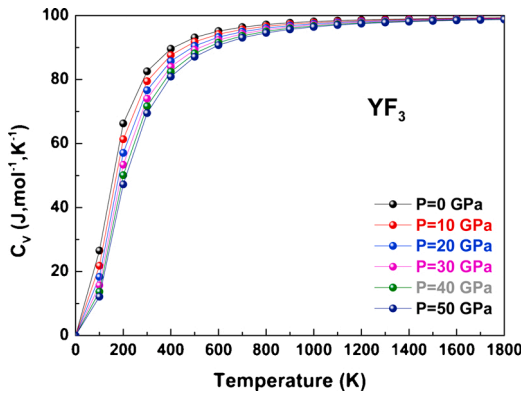

Fig. 13. The constant volume heat capacity as a function of temperature for YF_3 at different pressures.

represent the constants volume and pressure heat capacities C_V and C_P, respectively, as a function of temperature. Both C_V and C_P increase from 0 to 600 K and the difference between them is very slight. At sufficiently low temperature, C_V is proportional to T^3 [25]. At high temperature (T > 600 K) C_P follows on a very gradual linear increase, whereas C_V tends to the classical Petit and Dulong limit 99.2 $Jmol^{-1}K^{-1}$ [26]. C_V and C_P are 82.56 $Jmol^{-1}K^{-1}$ and 83.59 mol^{-1} K^{-1} at zero pressure and 300 K. Fig. 15 represents the temperature dependence of entropy S. The entropy is 73.76 $J.\ mol^{-1}\ K^{-1}$ at zero pressure and 300 K for YF_3. The predicted constants volume

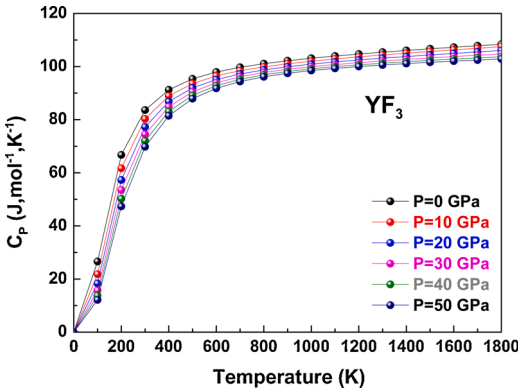

Fig. 14. The constant pressure heat capacity versus temperature for YF_3 at different pressures.

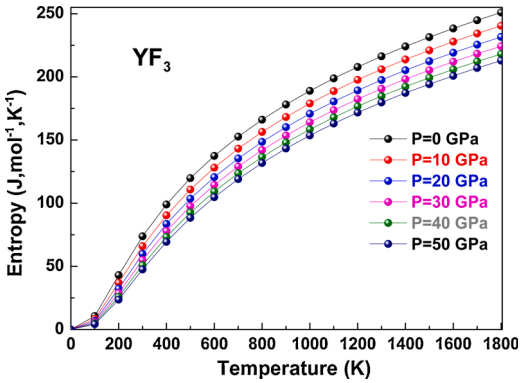

Fig. 15. The entropy as a function of temperature for YF_3 at different pressures.

Table 7
The predicted constant pressure heat capacity and entropy using GGA-PBE for YF_3.

Temperature (K)	C_P ($J.\ mol^{-1}K^{-1}$)		S ($J.\ mol^{-1}K^{-1}$)	
	This work	Experiment [27]	This work	Experiment [27]
0	0		0	
100	26.57		10.58	
200	66.72		43.03	
300	83.59	87.169	73.76	89.239
400	91.23	96.161	98.98	115.730
500	95.35	100.412	119.82	137.695
600	97.91	102.796	137.42	156.231
700	99.70	104.299	152.67	172.198
800	101.07	105.333	166.09	186.197
900	102.17	106.093	178.06	198.649
1000	103.11	106.684	188.88	209.859
1100	103.95	107.164	198.75	220.050
1200	104.70	107.568	207.83	229.392
1300	105.40	107.92	216.23	238.016
1400	106.06		224.07	
1500	106.68		231.41	
1600	107.27		238.31	
1700	107.83		244.82	
1800	108.37		251.01	

and constant pressure heat capacities and entropy obtained via QHDM with GGA-PBE for YF_3 are listed in Table 7 and compared with available experimental data [27].

4. Conclusions

We have studied physical properties of YF_3 using the PP-PW method based on the density functional theory within GGA-PBE, GGA-PBESOL and LDA. The lattice constant and bulk modulus calculated at equilibrium are in good agreement with theoretical data. The elastic moduli follow almost linear pressure dependence. Shear and Young's moduli and Poisson's ratio are estimated in the framework of the Voigt-Reuss-Hill approximations. The anisotropies in the mechanical properties have been explored. YF_3 in the cubic phase possesses small elastic anisotropy. Compared to isostructural metallic binaries [28], the elastic constants of YF_3 are significantly lower. This implies that YF_3 is fairly soft and damage tolerant. The high value of the absorption coefficient indicates that YF_3 is a potential candidate as a photocatalyst. The compound is a poor reflector of electromagnetic wave and therefore, has the prospect to be used as an anti-reflection coating material. The threshold energy of the dielectric function 5.15 eV corresponds to the fundamental direct band gap Γ-Γ. The computed thermodynamic parameters at different pressures and temperatures show canonical behaviors and agree quite well with experimental results where available.

Declaration of Competing Interest

The authors declare that the research was conducted in the absence of any commercial or financial relationships that could be construed as a potential conflict of interest

References

[1] D.F. Bezuidenhout, K.D. Clarke, R. Pretorius, Thin Solid Films 155 (1, 15) (1987) 17–30.
[2] Miao Wang, Qing-Li Huang, Jian-Ming Hong, Xue-Tai Chen, Mater. Lett. 61 (10) (2007) 1960–1963.
[3] Xiaoliang Yang, Siguo Xiao, J.W. Ding, X.H. Yan, J. Appl. Phys. 103 (9) (2008), https://doi.org/10.1063/1.2903582, 093101-093101-5.
[4] R.H. Nafziger, R.L. Lincoln, N. Riazance, J. Inorg. Nucl. Chem. 35 (2) (1973) 421–426.
[5] S.J. Clark, M.D. Segall, C.J. Pickard, P.J. Hasnip, M.J.P. robert, K. Refson, M.C. Payne, Zeitschrift fûr Kristallographie 220 (5–6) (2005) 567.
[6] D. Vanderbilt, Phys. Rev. B 41 (1990) 7892.
[7] J.P. Perdew, K. Burke, M. Ernzerhof, Phys. Rev. Lett. 77 (1996) 3865.
[8] S. Goedecker, M. Teter, J. Hutter, Phys. Rev. B 54 (1703) (1996).
[9] H.J. Monkhorst, J.D. Pack, Phys. Rev. B 13 (1976) 5188.
[10] T.H. Fischer, J. Almlof, J. Phys. Chem. 96 (1992) 9768.
[11] H.R. Jappor, Z.A. Saleh, M.A. Abdulsattar, Adv. Mater. Sci. Eng. 2012 (2012) 1.
[12] M.A. Blanco, A.M. Pendás, E. Francisco, J.M. Recio, R. Franco, J. Molec. Struct. Theochem. 368 (1996) 245.
[13] M. Flórez, J.M. Recio, E. Francisco, M.A. Blanco, A.M. Pendás, Phys. Rev. B 66 (2002), 144112.
[14] H.R. Jappor, Eur. J. Sci. Res. 59 (2011) 264.
[15] E. Francisco, M.A. Blanco, G. Sanjurjo, Phys. Rev. B 63 (2001), 049107.
[16] Kristin Persson, Materials Data on YF_3 (SG221) by Materials Project, 2014, https://doi.org/10.17188/1269248. United States: N. p.,Web.
[17] A.K. Kushwahaa, S.P. Mishra, M.K. Vishwakarma, S. Chauhan, H.R. Jappor, R. Khenata, S. Bin Omran, Inorg. Chem. Commun 127 (2021), 108495.
[18] W. Voigt, Lehrbuch Der Kristallphysik, Vieweg +Teubner Verlag, Wiesbaden, 1966, https://doi.org/10.1007/978-3-663-15884-4.
[19] A. Reuss, Berechnung der fließgrenze von mischkristallen auf grund der plastizitatsbedingung für einkristalle, ZAMM - Zeitschrift für Angew Math Und Mech 9 (1929), 49e58, https://doi.org/10.1002/zamm.19290090104.
[20] R. Hill, The elastic behaviour of a crystalline aggregate, Proc. Phys. Soc. 65 (1952), 349e54, https://doi.org/10.1088/0370-1298/65/5/307.
[21] A. Gencer, G. Surucu, Electronic and lattice dynamical properties of Ti_2SiB MAX phase, Mater. Res. Express 5 (2018), 076303, https://doi.org/10.1088/2053-1591/aace7f.
[22] R. Gaillac, P. Pullumbi, F.-X. Coudert, ELATE: an open-source online application for analysis and visualization of elastic tensors, J. Phys. Condens. Matter 28 (2016), 275201, https://doi.org/10.1088/0953-8984/28/27/275201.
[23] Md.Maruf Mridha, S.H. Naqib, Phys. Scr. 95 (2020) 105809, https://doi.org/10.1088/1402-4896/abb968.
[24] G. Berning PHH, R.P. Madden, JOSA 50 (1960) 586–597.
[25] P. Debye, Ann. Phys. 39 (1912) 789.
[26] A.T. Petit, P.L. Dulong, Ann. Chim. Phys. 10 (1819) 395.
[27] I. Barin, Thermodynamical Data of Pure Substances, third ed., VCH, New York, 1995.
[28] M.I. Naher, F. Parvin, A.K.M.A. Islam, S.H. Naqib, Eur. Phys. J. B 91 (2018) 289.